Journal of Alloys and Compounds 503 (2010) 177–185

Contents lists available at ScienceDirect

Journal of Alloys and Compounds

journal homepage: www.elsevier.com/locate/jallcom

Three-dimensional multispecies current density simulation of molten-salt electrorefining

Sungyeol Choi[a,*], Jaeyeong Park[a], Kwang-Rag Kim[b], HyoSook Jung[a], IlSoon Hwang[a], ByungGi Park[c], KyungWoo Yi[d], Han-Soo Lee[b], DoHee Ahn[c], Seungwoo Paek[c]

[a] Department of Nuclear Engineering, Seoul National University, Sillim-dong, Gwanak-gu, Seoul, 151-742, Republic of Korea
[b] Korea Atomic Energy Research Institute, 1045 Daedeok-daero, Yuseong-gu, Daejeon, 305-353, Republic of Korea
[c] Soonchunhyang University, Sinchang-myeon, Asan-si, Chungcheongnam-do, 336-745, Republic of Korea
[d] School of Materials Science and Engineering, Seoul National University, Sillim-dong, Gwanak-gu, Seoul, 151-742, Republic of Korea

ARTICLE INFO

Article history:
Received 6 March 2010
Received in revised form 30 April 2010
Accepted 30 April 2010
Available online 6 May 2010

Keywords:
Pyroprocessing
Electrorefining
Computational modeling
Spent nuclear fuel
Current density

ABSTRACT

This study presents three-dimensional simulation results of multispecies and multi-reaction electrorefining for spent nuclear waste treatment. Fluid-dynamic behavior of electrorefining is analyzed by commercial computational fluid-dynamics code. The results of local fluid dynamics are coupled with one-dimensional electrochemical reaction analysis code in order to predict local current density distribution. The new approach shows current distribution patterns over the cathode surface in LiCl–KCl molten-salt electrolyte. The current density distribution patterns are analyzed for various electrode rotational speeds and diverse applied currents and the results show a good agreement with general principle of mass transfer observations. Spatially periodic and vertically striped pattern of current density is predicted at the cathode side due to mass transfer depression at separation points. These slow mass transfer regions are vulnerable to be contaminated by transuranic elements. High rotational cathode speed and slow rotational anode speed are favorable to achieve uniform current density distribution with high applied current. The developed three-dimensional simulation will provide an improved understanding of complex electrochemical and transport phenomena that cannot be experimentally investigated and can be used to improve efficiency of electrorefiner design with high uranium throughput and small effluence of radioactive transuranic elements.

1. Introduction

The past 50 years operation of nuclear power plants has accumulated huge amounts of spent nuclear fuel (SNF) which retains high radioactivity and requires significantly long management periods. SNF is undeniable problem needed to be overcome for developing sustainable nuclear energy mechanism. Considering the opposition of the public to SNF and long management periods creating large uncertainty, SNF should be removed through environmental-friendly technical and institutional approaches. These approaches should have proliferation resistance that is critical to the future viability of the nuclear energy [1].

The Argonne National Laboratory (ANL) has developed pyroprocessing to solve SNF issue [2,3]. Pyroprocessing is proliferation-resistant technology to recover uranium, transuranic elements (TRU), and long-lived fission products (LLFP) from SNF in order to reutilize them for fast reactor fuels or transmutation targets. This technology can considerably reduce the volume and the toxicity of radioactive waste. Metallic SNF of EBR-II was investigated and treated by pyroprocessing in the Idaho National Laboratory (INL) and the ANL [4,5]. In pyroprocessing, electrorefining plays an important role to recover uranium over 99% from metallic spent fuel mixture. However, it is difficult to achieve a high uranium throughput with high decontamination factor (>100) without TRU contamination because of the nature of strong tendencies for non-uniform mass transfer rate. In order to improve the uniformity of mass transfer and optimize electrorefining performance, computational analysis is necessary to predict three-dimensional electro-fluid behavior.

In this paper, three-dimensional results of local current density distribution are calculated for various electrode rotational speeds and applied currents based on the Mark-IV electrorefiner developed and operated by the INL. The vessel of the Mark-IV is composed of stainless steel with the inner diameter of 100 cm, two anodes, and one cathode and it contains LiCl–KCl eutectic molten electrolyte [6]. The set of equations for fluid dynamics is solved through commercially available computational fluid-dynamics (CFD) code whose solution methodology is schemed on

* Corresponding author. Tel.: +82 2 880 7200; fax: +82 2 3285 9600.
E-mail address: choisys7@snu.ac.kr (S. Choi).

0925-8388/$ – see front matter © 2010 Elsevier B.V. All rights reserved.
doi:10.1016/j.jallcom.2010.04.228

Nomenclature

A	electrode area (cm^2)
C	concentration as a function of location and time (mol/cm^3)
C^*	bulk concentration of electro-active species (mol/cm^3)
C^o	surface concentration of electro-active species at the electrode (mol/cm^3)
d	diameter of rotating cylindrical cathode (cm)
D	diffusion coefficient of electro-active species (cm^2/s)
F	Faraday constant (96,485 C/mol)
i_o	exchange current density (A/cm^2)
i^C	cathode current density (A/cm^2)
i^A	anode current density (A/cm^2)
i_{app}	applied current density at the electrode (A/cm^2)
I	current (A)
M	mass fraction of actinide in the LiCl-KCl electrolyte
$\dot{m}$	mass flux at electrode surface (kg/cm^2 s)
M_U	molar mass of uranium (kg/mol)
n	normal direction to surface
N	mass flux of electro-active species (kg/cm^2 s)
P	pressure (Pa)
R	universal gas constant (J/mol K)
Re	Reynolds number ($Re = Ud/\mu$)
S_c	mass source and sink
Sc	Schmidt number ($Sc = \mu/D$)
S_u	momentum source for forced convection such as electrolyte stirring
t	time (s)
T	temperature (K)
u	mobility of ion (cm^2/V s)
U	peripheral velocity of rotating cylinder electrode (cm/s)
v	velocity (cm/s)
z	number of electrons in the electrode reaction

Greek letters

Φ	electrical potential (V)
α	symmetric constant
δ	Nernst diffusion boundary layer thickness (cm)
η	concentration overpotential (V)
μ	kinematic viscosity (cm^2/s)
ρ	density (kg/cm^3)

the finite-volume discretization [7]. The electro-transport behavior is analyzed by coupling three-dimensional fluid dynamics with multispecies current density correlations generated from one-dimensional electrochemical reaction code.

Similar researches were studied in copper electroplating and flow accelerated corrosion fields [8–10]. These studies show that local mass transfer effect in turbulent condition is generally difficult to understand because turbulent flow has typical irregularities and extremely thin diffusion boundary layer at high Sc number condition ($Sc \approx 720$ in this study) [11]. Although modeling limitation for large commercial scale equipments and difficulties at high Sc number condition, it is believed that three-dimensional simulation will provide an improved understanding of complex electrochemical and transport phenomena that cannot be experimentally investigated.

2. Theory of electrorefiner modeling

2.1. Purpose of electrorefiner modeling

In pyroprocessing, electrorefining is a cardinal step to recover depleted uranium from SNF [12]. Electrorefining is composed of three steps from material dissolution at the anode to material deposition at the cathode. The first step is the dissolution of uranium, TRU and other elements as an ionic form into LiCl–KCl molten-salt electrolyte. The second step is the transport of cations through the electrolyte toward the cathode surface. The final step is that uranium is reduced and deposited as a metallic form at the cathode surface [13]. These processes are strongly coupled with complicate electrochemical kinetics, electrochemical thermodynamic, and ion transport phenomena [14].

Electrorefiner design goal is the maximization of uranium recovery rate without undesired TRU yield. Uranium throughput is determined by electrorefiner geometry, the chemical state of electrolytic cell, and operating conditions such as mixing effect, applied current, and cell voltage [15]. Uranium in final waste stream from pyroprocessing should be decontaminated with TRU for reducing radioactive hazard and management periods [16]. To increase process throughput and prevent local TRU deposition at the cathode, it is important to achieve high applied current with uniform distribution. Non-uniform current density distribution can arise when cathode deposition is controlled by mass transfer rate of one or more electro-active species and this mass transfer is spatially non-uniform over the electrode surface [10].

Numerous researches for one- or two-dimensional electrorefiner modeling have been studied and these approaches show a good agreement with experimental data [14,17–21]. However, geometrical and compositional non-uniformity cannot be estimated by one- or two-dimensional simulation code. Three-dimensional electrorefiner modeling has to be adopted to design favorable electrorefiner geometry and determine effective operational conditions.

2.2. Difficulties of three-dimensional multispecies current density modeling

Three-dimensional modeling of multispecies current density in both steady state and transient conditions has the following difficulties:

1. Extremely expensive computational resources are required for both steady state and transient analysis.
2. Time interval has to be very small due to rapid changes of the rate of deposition and dissolution in transient simulation.
3. In actual electrorefining, steady state does not exist because dissolved and deposited species are continuously changed.
4. Geometrical changes with cathode deposition and anode dissolution are difficult to simulate in transient modeling.
5. Species concentration rapidly varies near the electrode surface, which requires extremely fine mesh size within 10^{-4} m from the electrode surface.
6. Complicated geometry of electrorefiner can cause convergence problem.
7. Diffusion and migration of materials in solid are difficult to simulate.

In this study, it is assumed that uranium species dominates overall fluid-dynamic behavior of electrorefining. Three-dimensional steady state was simulated and its results are converted to local multispecies current density distribution by coupling with one-dimensional electrochemistry code.

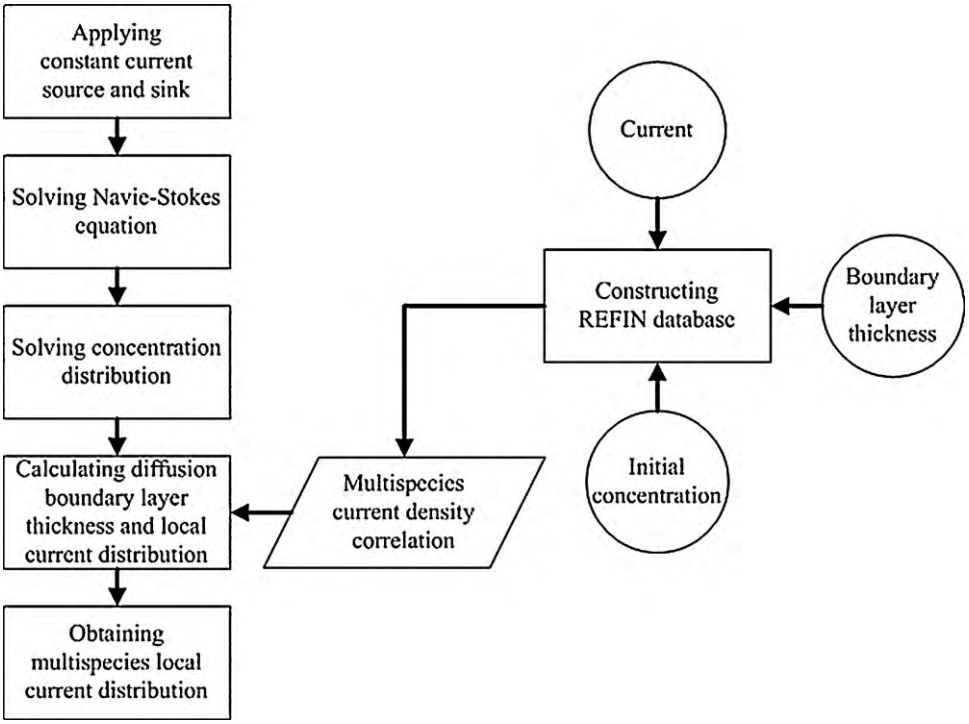

Fig. 1. Overall electrorefiner modeling approach for multispecies and multi-reaction.

2.3. Analysis tool and procedure

Overall electrorefiner modeling approach for multispecies and multi-reactions is shown in Fig. 1. Analysis tool consists of one-dimensional electrochemical reaction simulation code, *REFIN*, and three-dimensional CFD code [12]. *REFIN* has been developed to solve the time-dependent simulation of molten-salt electrolysis within diffusion boundary layer for nuclear waste treatment. It is verified by the experiment of Tomczuk and co-workers [17,22]. *REFIN* can calculate multispecies current density, potential variation for each species and electrode, surface concentration and the amount of materials dissolution and deposition as a function of time [23]. CFD code solves three-dimensional flow velocity profile, concentration distribution of chemical species, and mass transfer behavior.

Detailed analysis procedure of electrorefiner modeling is as following:

1. Database of current density for uranium and TRU are constructed by using the simulation results of one-dimensional electrochemical code.
2. Current density correlations are generated as a function of applied current density, boundary layer thickness, and initial concentration of actinide.
3. For CFD simulation, constant current source and sink are respectively applied to the anode and the cathode. This analysis only considers uranium in molten salt as a representative element of actinide group.
4. Velocity profile is calculated from the solution of the Navier–Stokes equation.
5. Concentration distribution of electro-active species is solved from the concentration transport equation.
6. Local Nernst boundary layer thickness is calculated from concentration distribution results.
7. The boundary layer thickness indicates mass transfer rate at the local electrode surface and it is converted to local current.
8. The local actinide group currents are divided into uranium and TRU current by using current density correlations generated from *REFIN*.

2.4. Mathematical method

The ion transfer mechanism from anode source to cathode sink through molten-salt electrolyte is significant to understand electrorefining performance. Mass flux for each species is described by the combination of electromigration, diffusion and convection as shown in Eq. (1) [24].

$$N = -zuFC\nabla\Phi - D\frac{C^* - C^0}{\delta} + Cv \tag{1}$$

Mass transfer is dominated by convection in bulk electrolyte and by diffusion in diffusion boundary layer. The mass transfer effect near the electrode wall is treated by Nernst diffusion boundary layer and its thickness is generally very small compared to the electrode size [24,25].

For CFD analysis, steady, incompressible, isothermal and turbulent flow are assumed. Multi-component single phase behavior is calculated based on the continuity equation, the Navier–Stokes equation, and the mass transport equation represented, respectively, in Eqs. (2), (3), (4). Electromigration effect is assumed to be negligible compared to convection and diffusion. This approximation is appropriate in most electrorefining process with sufficient supporting electrolyte. Boundary condition is derived from constant current operation which is converted to mass source and sink based on Faraday's law as shown in Eq. (5). No slip and insulating boundary condition are applied at the walls as represented in Eq. (6), but top surface is treated as a free slip boundary condition [25–27].

$$\rho(\nabla \cdot v) = 0 \tag{2}$$

$$\rho\frac{\partial v}{\partial t} + \rho v\nabla v = -\nabla P + \mu\nabla^2 v + S_u \tag{3}$$

$$\rho\frac{\partial C}{\partial t} + \rho\nabla\cdot(\nu C) = \rho\nabla\cdot(D\nabla C) + S_c \quad (4)$$

$$\dot{m} = \pm\frac{iAM_U}{nF} \quad (5)$$

$$\frac{\partial C}{\partial n} = \frac{\partial \Phi}{\partial n} = 0 \quad (6)$$

The normal concentration gradient to the electrode surface is significantly larger than that of the lateral direction. It means that the normal concentration gradient to the electrode surface is controlling motion of mass transfer at the near electrode surface [17].

REFIN considers diffusion and electromigration within given diffusion boundary layer. Local reaction rate is expressed by modified Butler–Volmer equation with concentration depending terms as shown in Eq. (7) [17,28]. This means that for a lower surface concentration ($C^S < C^b$) at the electrode surface, a higher overpotential is necessary for satisfying the same current density.

$$i = i^o\left[\frac{C_O^S}{C_O^b}\exp\left(-\frac{\alpha F}{RT}\eta\right) - \frac{C_R^S}{C_R^b}\exp\left(\frac{(1-\alpha)F}{RT}\eta\right)\right] \quad (7)$$

2.5. Turbulent model

There are eddy-viscosity model including the k–ε model and the k–ω model, and Reynolds stress model in order to simulate turbulent flow and resolve the near wall velocity profile [9]. Reynolds stress model solves velocity profile in viscosity sub-layer by fully numerical method without any assumption or experimental correlation. However, it reduces numerical robustness and needs much smaller mesh resolution and longer simulation time than those of eddy-viscosity model. It is only appropriate to apply simple geometrical configuration such as straight pipe and smooth cylinder in low *Sc* and Reynolds number conditions [29]. Higher *Sc* numbers creates more contribution of turbulent transport to velocity profile and mass transfer near the electrode, which significantly requires extremely high resolution of mesh near wall region [25,30].

Eddy-viscosity model employs a wall function approach combined with empirical formulas to simulate near wall behavior. The k–ε model uses a convectional wall function approach but is not sufficient to recognize rapid variations of species velocity and concentration profile at the relatively high *Sc* number condition. The reason is that diffusion layer at high *Sc* number is much thinner than velocity layer. According to several literatures, the k–ω model was found to have better capability of close to wall behavior simulation than that of the k–ε model [26]. As an improvement version of the k–ω model, shear stress transport (SST) model, developed for accurate boundary layer simulation, is used to predict turbulent flow in this simulation. SST model adopts the low-Reynolds-number method (i.e., low turbulent Reynolds number in viscous sub-layer) to solve rapid variation near wall region [31,32].

3. Results and discussion

3.1. Generation for multispecies current density correlations

Multispecies current density distributions are influenced by applied current, diffusion boundary layer thickness, and initial nuclide concentration in molten-salt electrolyte. Based on these influencing parameters, correlations for uranium and neptunium current density are produced at both the anode and the cathode as shown from Eq. (8) to Eq. (11). Neptunium is suddenly deposited at the cathode, when cathode potential becomes more negative than neptunium equilibrium potential under the given conditions. For modeling this sudden arise of neptunium current, unit step function is adopted in neptunium cathode current density correlation.

Table 1
Initial operating conditions for total current of 80 A.

Location	Initial mass flux (kg/m^2 s)
Anode 1	1.20×10^{-4}
Anode 2	1.20×10^{-4}
Cathode side	3.47×10^{-4}
Cathode bottom	3.47×10^{-4}

$$i_U^C = (0.999 + (-65M + 0.2)\times U(\delta - 0.25M + 0.005) \times (\delta - 0.25M + 0.005))i_{app} \quad (8)$$

$$i_{Np}^C = \frac{1.2655M + 0.11954}{200(\delta - 0.25M)\times U(\delta - 0.23075M + 0.00056) + 1} \times U(\delta - 0.23075M + 0.00056)\times U(i_{app} - 0.2644 + 14.7212\delta - 3.6903M)\times(i_{app} - 0.2644 + 14.7212\delta - 3.6903M) \quad (9)$$

$$i_U^A = (0.000054 - 0.000185\delta - 0.00277M + 0.019481\delta M) \times i_{app}^{-1.24229-3.84338\delta+3.47382M+20.5332\delta M} \quad (10)$$

$$i_{Np}^A = (0.03679 + 0.0091885M + 0.01123\delta + 0.061403\delta M)\times i_{app} \quad (11)$$

Current density correlations are first derived as a function of applied current density which is evaluated to the most sensitive parameter. Second, its coefficients are modified to accept the effects of diffusion boundary layer thickness and initial mass fraction. These correlations cover applied current density ranged from 0.02 to 0.3 A/cm^2 and boundary layer thickness varied from 0.001 to 0.02 cm. Initial concentration of actinide is validated in mass fraction ranged from 0.04 to 0.08 in molten-salt electrolyte. The correlations show a good agreement with *REFIN* calculation results as shown in Fig. 2. In extreme condition with high applied current density and large diffusion boundary layer thickness, the correlation of cathode neptunium current density does not correspond with *REFIN* calculation results due to the increase of lanthanide current. However, its threshold points for cathode deposition are well matched with *REFIN* results, which is sufficient to decide whether TRU deposition occurs or not because neptunium is the first reduced element in TRU.

3.2. Three-dimensional electrolyte fluid analysis

Table 1 shows initial operating conditions and geometrical information of the Mark-IV electrorefiner [15,33]. Cd pool at the bottom is ignored with the assumption of small mass transfer contribution in electrorefining for simplicity in fluid-dynamics modeling. This assumption is acceptable for the process with electrically disconnected liquid Cd pool. Table 2 contains material properties of LiCl–KCl molten-salt electrolyte for fluid-dynamics analysis [13,34]. The operating condition does not reach limiting current condition with initial actinide mass fraction of 0.08.

Fig. 3 shows streamlines from two anodes and color indicates flow speed. Two anodes and one cathode rotate in a counter clock-

Table 2
Material properties of LiCl–KCl molten-salt electrolyte.

Data	Value
Molar mass (g/mol)	68.121
Density (g/cm^3)	1.551
Dynamic viscosity (N s/m^2)	0.00123
Operating temperature (K)	773

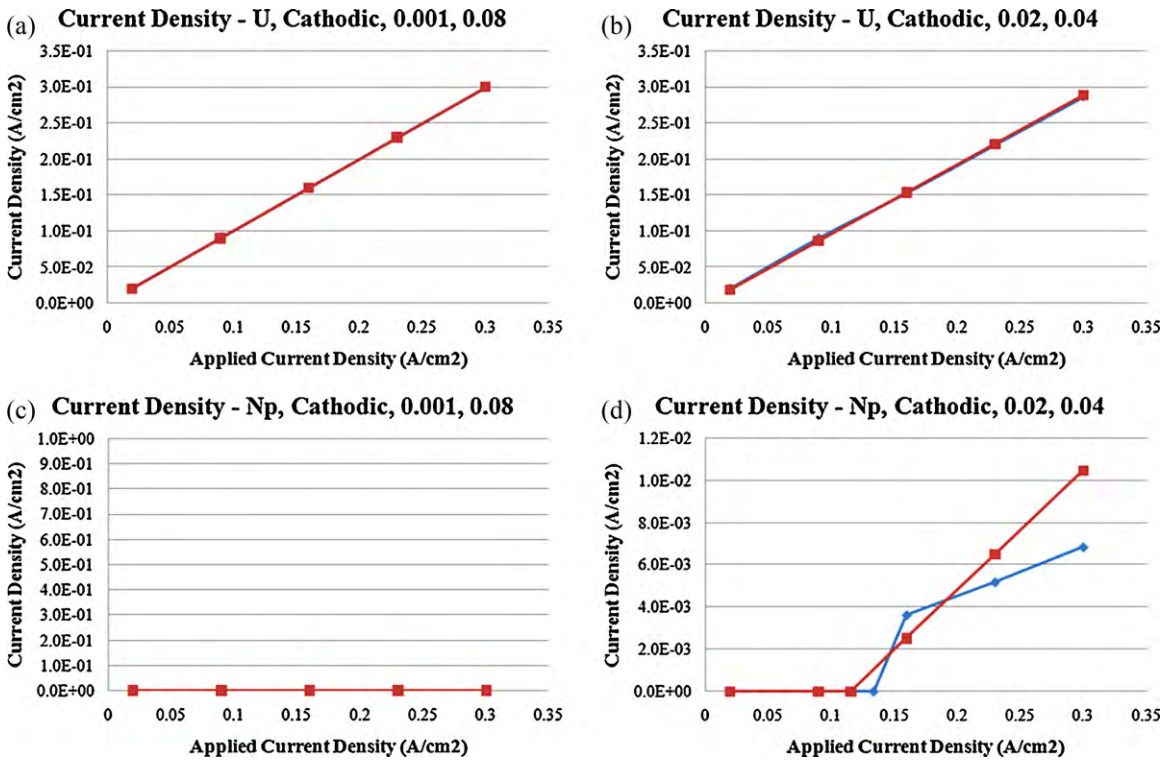

Fig. 2. Cathode current density for uranium and neptunium: red – correlation and blue – *REFIN* calculation (δ = 0.001, 0.02 cm and bulk mass fraction of actinide = 0.04, 0.08). (For interpretation of the references to color in this figure legend, the reader is referred to the web version of the article.).

wise direction with various electrode rotating speeds. Shaft at the center of electrorefiner rotates in a clockwise direction with rotational speed of 20 rpm. The high resolution mesh with the minimum size of 10^{-7} m at the electrode wall is used to simulate rapid variation of species concentration and turbulent behavior near the electrode wall.

Average concentration profile from the electrode surface is represented in Figs. 4 and 5. Both the cathode side and bottom show well developed concentration profile. In the high rotational speed case, bulk concentration reaches close to the electrode and inconsiderable uranium concentration drop is estimated. In addition, diffusion boundary layer thickness becomes smaller with the increase of electrode rotational speed, which enhances mass transfer rate of ion species to the cathode.

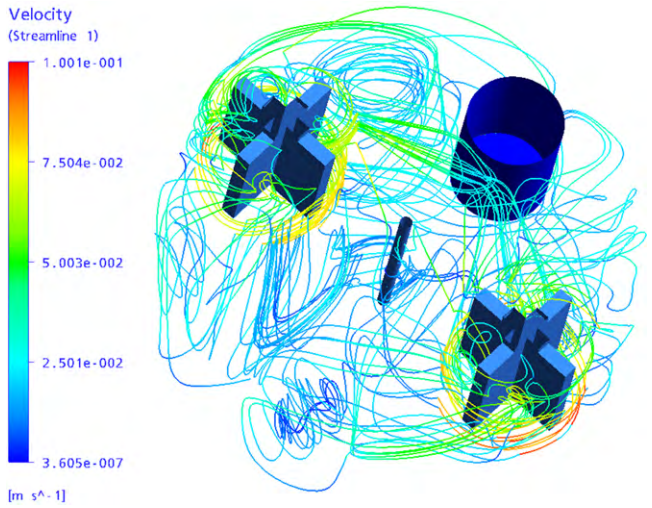

Fig. 3. Streamline for Mark-IV electrorefiner (80 A, 5 rpm of electrode rotating speed).

Velocity prolife is shown in Fig. 6 for various electrode rotational speeds. All cases show that downward flow is formed near the cathode side and flow velocity decreases at location in the lower height. The fluid is axially sucked towards the cathode bottom and thrown radial outwards. Special cross-shape of anodes and rotational cathode motion form complicated local vortex flow and global circulation loop. These fluctuation velocity components result in a significant variation of surface mass transfer [31,35].

Local diffusion boundary layer thickness is directly related to local current distribution which is shown in Figs. 7 and 8. These two figures represent actinide group current density calculated by three-dimensional electro-fluid-dynamic simulation of uranium. Spatially periodic and vertically striped pattern of current density is predicted at the cathode side. Striped pattern becomes more noticeable with increasing rotational speed as shown in Fig. 7.

There are two competing effects of current density distribution with the increase of rotational speed. One effect is the rise of cross-flow intensity across the cathode with the intensity of rotational anode motion. Faster rotational anode motion generates larger cross-flow intensity across the cathode from several different directions as shown in Fig. 9, which increases the irregularity of flow behavior and decreases current density uniformity around the cathode side. Velocity profile near the cathode is getting more irregular as rotational speed increases. According to previous experimental results, a rotating cylindrical electrode without cross-flow generally shows fairly uniform mass transfer rate. However, rotating cylindrical electrode with higher cross-flow intensity shows more prominent non-uniformity of mass transfer rate because of mass transfer depression at separation points [36].

Another effect is the increase of uniformity of mass transfer by rotational cathode motion. Increasing cathode rotation speed makes current density distribution more uniform which well cor-

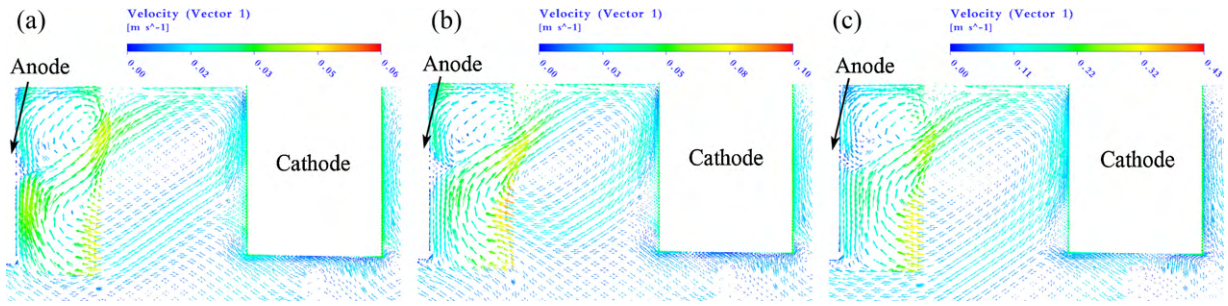

Fig. 4. Molar concentration distribution with rotating speed (normal direction from the cathode side).

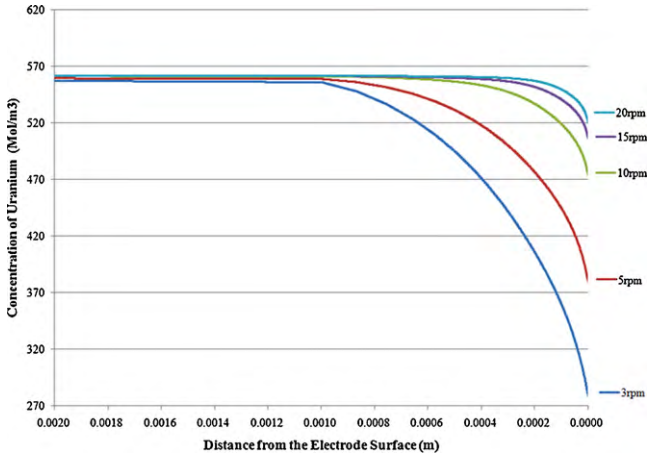

Fig. 5. Molar concentration distribution with rotating speed (normal direction from the cathode bottom).

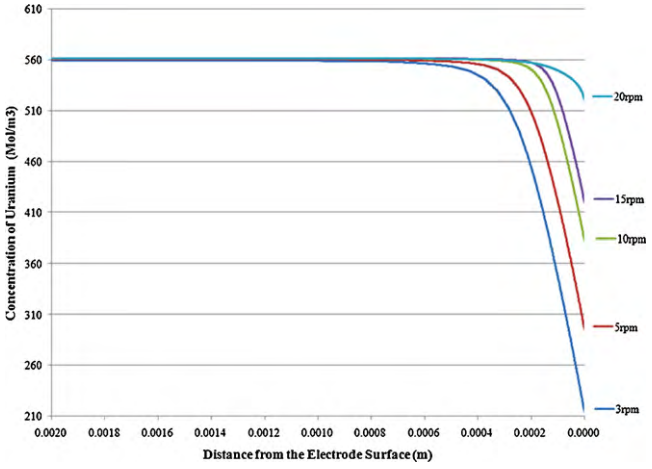

Fig. 6. Vertical velocity profile between anode and cathode in total applied current of 80 A (a) 3 rpm, (b) 5 rpm, (c) 20 rpm.

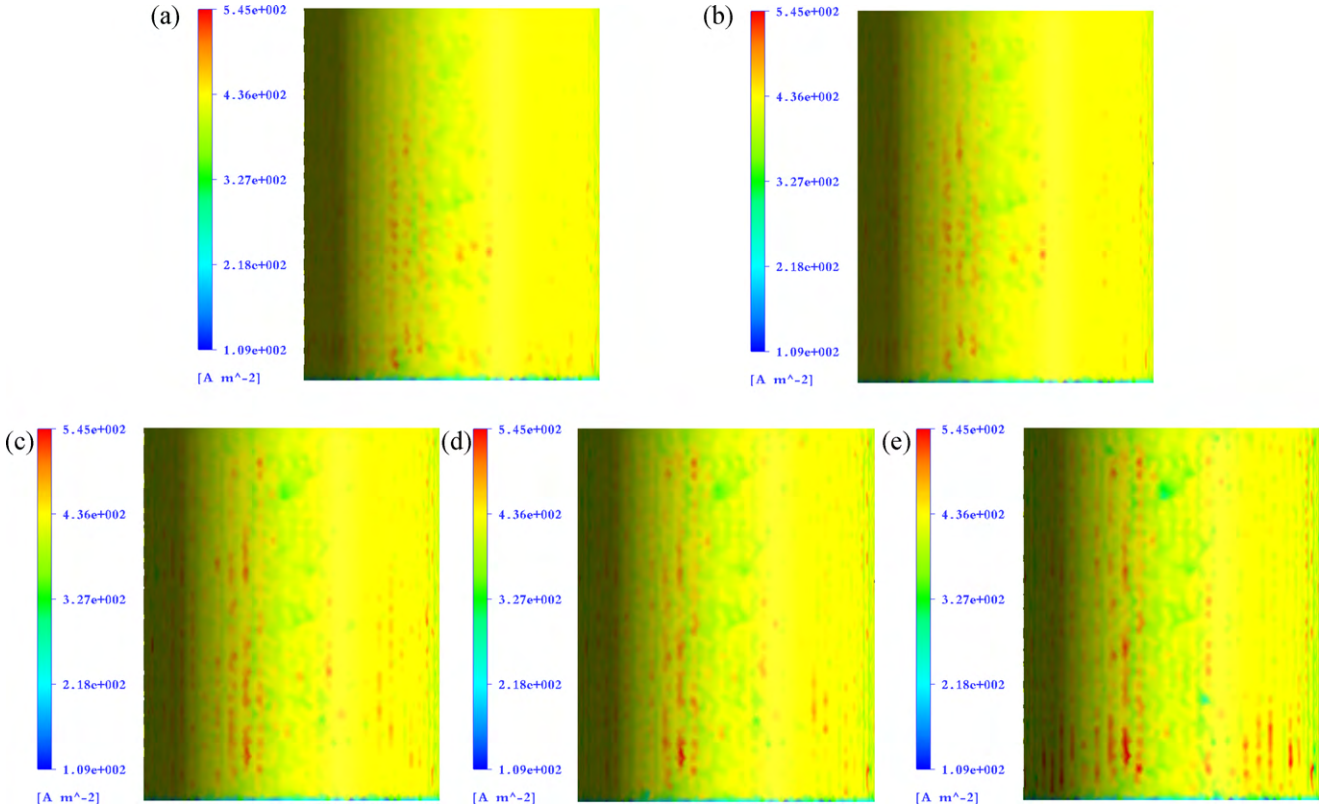

Fig. 7. Current density distribution at the cathode side for the various rotating speed with mass fraction of 0.08 (a) 3 rpm, (b) 5 rpm, (c) 10 rpm, (d) 15 rpm, (e) 20 rpm.

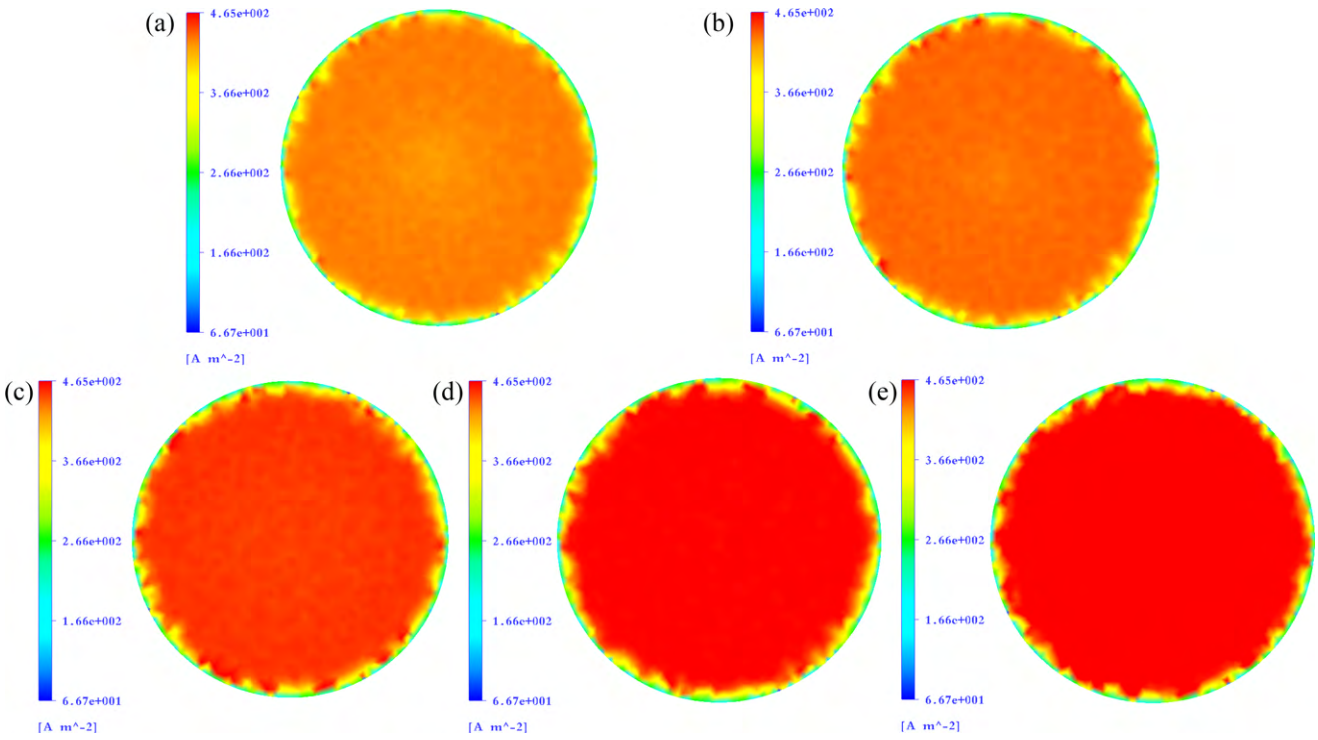

Fig. 8. Current density distribution at the cathode bottom for the various rotating speed with mass fraction of 0.08 (a) 3 rpm, (b) 5 rpm, (c) 10 rpm, (d) 15 rpm, (e) 20 rpm.

responds with previous experiment results [36]. The reason is that cross-flow near the cathode is dispersed as rotational cathode speed increases. In this simulation, the non-uniform effect of the anode motion overwhelms the uniform effect by the cathode motion. High rotational cathode speed and slow rotational anode speed are favorable to achieve uniform current density distribution with high applied current within acceptable economic criteria of cooling equipments.

3.3. Multispecies current density analysis

Actinide local current density, local diffusion boundary layer thickness, and initial mass fraction of actinide elements are applied to generated multispecies correlations as input parameters. Fig. 10 respectively represents neptunium current density at both the cathode side and bottom for various electrode rotational speeds. As uranium in molten salt is exhausted or cannot satisfy applied current, overpotential rises to find second reduction reaction and other species begin to deposit at the cathode surface [12]. At the low rotational speed, local neptunium deposition occurs at the edge of cathode side and bottom where materials are separated from the electrode surface. Increasing rotational speed produces effective mass transfer behavior at the whole cathode surface and bulk concentration reaches to the close wall that is thin diffusion boundary layer thickness and increased tolerance of limiting current. Hence, local deposition of neptunium disappears at the high rotational speed of the electrode as represented in Fig. 10.

Fig. 11 shows neptunium current distribution at the cathode side and bottom for the various applied currents at rotational speed of 3 rpm and the initial mass fraction of 0.04. As applied current increases, neptunium current proportionally rises and widely spreads over the cathode surface. Small initial mass concentration in molten salt is vulnerable to be contaminated neptunium or other TRU because uranium cannot satisfy high current density. It means that it is important to effectively determine optimized termination condition of electrorefining. Excessive recovery yield of uranium

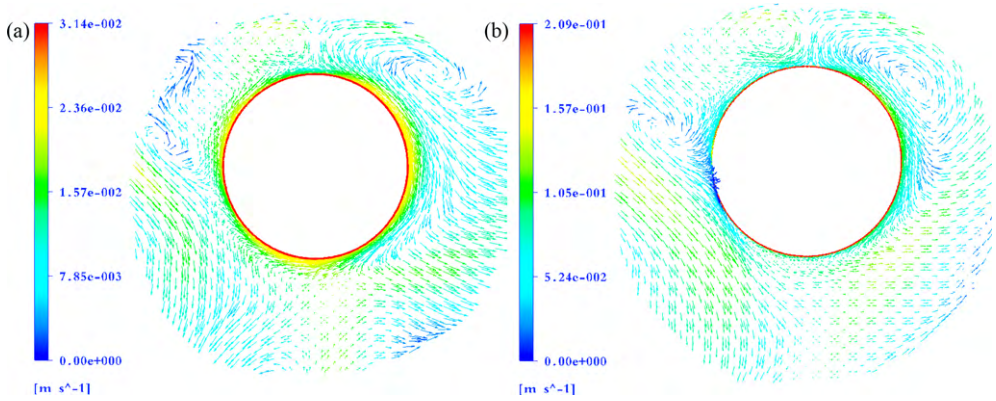

Fig. 9. Horizontal velocity profile between the anode and the cathode in total applied current of 80 A (a) 3 rpm, (b) 20 rpm.

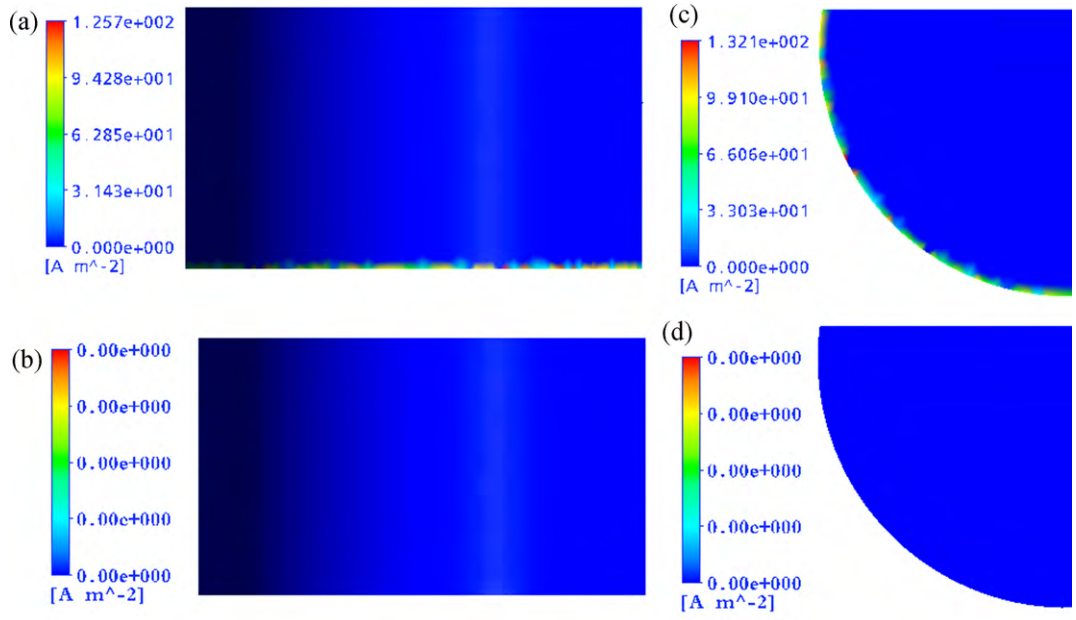

Fig. 10. Neptunium current density distribution at the cathode side and bottom for the various rotating speed with mass fraction of 0.08 (a) 0 rpm, (b) 10 rpm at cathode side and (c) 0 rpm, (d) 15 rpm at cathode bottom.

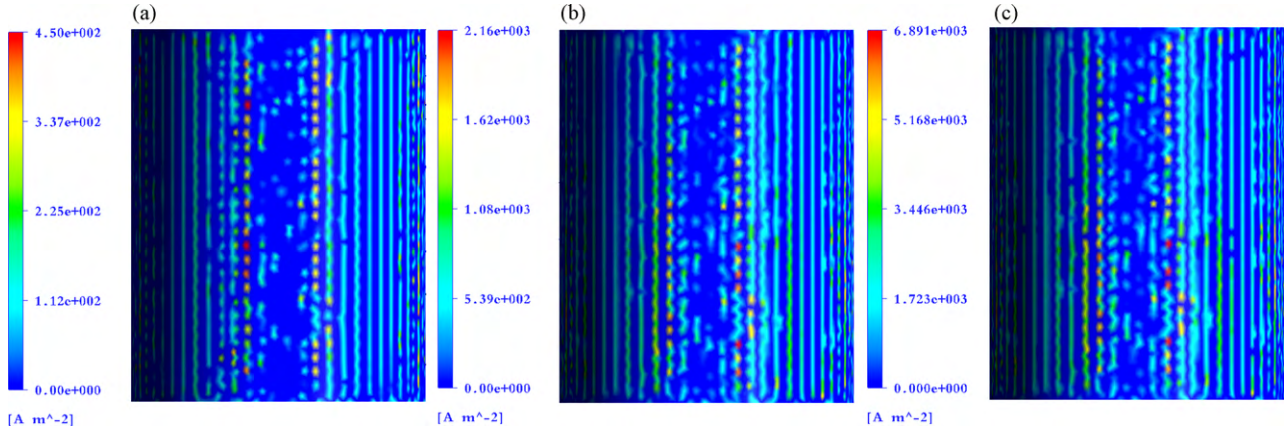

Fig. 11. Neptunium current density distribution at the cathode bottom for the various applied current at 3 rpm with mass fraction of 0.04 (a) 80 A (b) 120 A (c) 160 A.

may result in unsuitable TRU deposition and sufficient amount of uranium ion in molten salt should be maintained during electrorefining of spent nuclear fuel.

4. Conclusions

A three-dimensional multispecies and multi-reaction modeling approach is developed for electrorefining to treat spent nuclear fuel. Electro-fluid-dynamic behavior is analyzed by the coupling of one-dimensional electrochemical reaction analysis code and three-dimensional CFD code. The approach provides the information of local concentration distribution and local multispecies current density distribution. This result shows design strategies of effective electrorefiner which satisfies high uranium throughput without TRU yield. The current density distribution patterns are analyzed for various electrode rotational speeds and diverse applied currents and the results show a good agreement with general principle of mass transfer observations. Future work will focus on the development of correlations for other TRU and conduct a benchmark testing for developed approach with available aqueous experiments such as rational cylindrical hull cell [37].

Acknowledgements

This work was supported by Nuclear Research & Development Program of the Korea Science and Engineering Foundation (KOSEF) grant funded by the Korean government (MEST).

This work was performed for International Nuclear Energy Research Initiative (INERI) program with the Republic of Korea and the United State government through the Korea Atomic Energy Research Institute (KAERI) and the Idaho National Laboratory (INL).

References

[1] M. Benedict, T.H. Pigford, Nuclear Chemical Engineering, second ed., McGraw-Hill, 1981.
[2] J.J. Laidler, et al., Progress in Nuclear Energy 12 (1997) 131.
[3] Y.I. Chang, Nuclear Technology 88 (1989) 129.
[4] R.W. Benedict, et al., ANS Transaction 77 (1997).
[5] J.P. Ackerman, et al., Progress in Nuclear Energy 12 (1997) 141.
[6] S.X. Lia, et al., Journal of New Materials for Electrochemical Systems 3 (2000) 259.
[7] ANSYS, ANSYS CFX-Solver Theory Guide, ANSYS, Inc., Canonsburg, 2006.
[8] L.A. Gochberg, J.C. Sheu, et al., 207th Meeting of the Electrochemical Society, Electrochemical Society, Quebec City, Canada, 2005.
[9] C. Davis, P. Frawley, Corrosion Science 51 (2009) 769.

[10] J.O. Dukovic, The IBM Journal of Research and Development 34 (1990) 693.
[11] J.-Y. Hwang, K.-S. Yang, KSME Journal 29 (2005) 837.
[12] K.R. Kim, et al., Journal of Radioanalytical and Nuclear Chemistry 280 (2009) 401.
[13] J. D. Bae, K.W. Yi, B.G. Park, I.S. Hwang, H.Y. Lee, Global 2005, Tsukuba, Japan, 2005.
[14] R. Hoover, et al., Journal of Engineering for Gas Turbines and Power 131 (2009).
[15] S.X. Li, D. Vaden, R.D. Mariani, T.A. Johnson, Embedded Topical Meeting Spent Fuel and Fissile Material, American Nuclear Society, San Diego, CA, 2000.
[16] S.I. Kim, Progress in Nuclear Energy 49 (2007) 14.
[17] B.G. Park, Department of Nuclear Engineering, Ph.D., Seoul National University, Seoul, 1999.
[18] J.P. Ackerman, Trans. Am. Nucl. Soc 60 (1989) 168.
[19] H.P. Nawada, et al., Journal of Nuclear Science and Technology 32 (1995) 1127.
[20] R.K. Ahluwalia, H.K. Geyer, Nuclear Technology 116 (1996) 180.
[21] T. Kobayashi, M. Tokiwai, Journal of Alloys and Compounds 197 (1993) 7.
[22] Z. Tomczuk, Journal of Electrochemical Society 132 (1992).
[23] B.G. Park, I.S. Hwang, The 195th Meeting of the Electrochemical Society, The Electrochemical Society, Seattle, 1999.
[24] A.J. Bard, L.R. Faulkner, Electrochemical Methods, Fundamentals and Applications, John Wiley & Son, Inc., New York, 2001.
[25] A. Filzwieser, K. Hein, G. Mori, Journal of the Minerals, Metals and Materials Society 54 (2002).
[26] M.J. Leahy, M.P. Schwarz, 16th Australasian Fluid Mechanics Conference, Gold Coast, Australia, 2007.
[27] M.-H. Chung, Electrochimica Acta 45 (2000) 3959.
[28] V. Boovaragavan, C.A. Basha, Journal of Applied Electrochemistry 36 (2006) 745.
[29] J.-Y. Hwang et al., Journal of Fluids Engineering, ASME, 2007.
[30] M. Bilson, K. Bremhorst, 3rd International Conference, CSIRO Australia, Melbourne, Australia, 2003.
[31] A. Spille-Kohoff, ANSYS Conference & 26th CADFEM Users' Meeting, Darmstadt, Germany, 2008.
[32] ANSYS, ANSYS CFX-Solver Modeling Guide, ANSYS, Inc., Canonsburg, 2006.
[33] S.X. Li, et al., 193rd Meeting of the Electrochemical Society XI-Eleventh International Symposium on Molten Salts, The Electrochemical Society, 1988.
[34] George J. Janz, NIST Properties of Molten Salt Database, 1992.
[35] A. Keating, A Model for the Investigation of Two-phase Erosion-Corrosion in Complex Geometries, MSc, University of Queensland, 1999.
[36] L. Labraga, T. Berkah, International Journal of Heat and Mass Transfer 47 (2004) 2493.
[37] C.T.J. Low, et al., Electrochimica Acta 52 (2007) 3831.

Glossary

ANL: Argonne National Laboratory
CFD: computational fluid dynamics
INL: Idaho National Laboratory
KAERI: Korea Atomic Energy Research Institute
LLFP: long-lived fission products
SNF: spent nuclear fuel
SST: shear stress transport
TRU: transuranic elements